Novel Methods for Solving Dual-Risk-based Optimal Power Flow

Bin-Yang Liu
School of Electrical and Information Engineering
Tianjin University
Tianjin, China

Hsiao-Dong Chiang, Fellow, IEEE
School of Electrical and Computer Engineering
Cornell University
Ithaca, NY, USA

***Abstract*—Modern power systems are increasingly subjected to dual risks from both the load and the generation sides. Load-side stressors like concentrated large loads can lead to severely fluctuating power flow distributions, while the low-inertia conditions, induced by high penetration of renewable energy from generation sides, introduce significant frequency regulation challenges. While various OPF extensions exist, a unified framework capable of flexibly managing these compound or dual contingencies remains an active research area. This paper proposes a risk-based ACOPF model that incorporates dual risks: branch power flow risk and system frequency response risk. Case studies on 9-bus and 39-bus systems indicate the capability of the dual-risk ACOPF model to navigate security-economic trade-offs and presents marginal risk cost, which quantify the economic impact between different security levels, providing system operators with a flexible tool to enhance robustness in frequency response and thermal limit mitigation while preserving economic efficiency.**

***Index Terms*-- Risk assessment, optimal power flow, power flow security, frequency security.**

I. Introduction

Optimal Power Flow (OPF) is a cornerstone of power system operations, with Security-Constrained OPF (SCOPF) enforcing the deterministic "N-1" criterion to ensure a baseline of reliability [1]. Although robust, it is primarily designed for a well-defined set of contingencies and does not inherently account for variations in the probability or severity of potential violations. This often leads to a dispatch that is more conservative than is economically optimal in systems with significant uncertainty. [2]. Furthermore, systems are exposed to high-impact, low-probability events, which are a key focus of resilience studies [3].

Probabilistic OPF (P-OPF) emerged to address these limitations by modeling uncertainties, evaluating security through metrics like violation probability [4]. However, P-OPF quantifies the likelihood of insecure events but does not focusing on modeling their consequences, creating a critical gap in risk management where a high-probability, low-impact event may be prioritized over a more severe, lower-probability one.

This evolution leads to Risk-Based OPF (RBOPF), which integrates contingency probability with operational impact [5]. Existing research bifurcates into two categories: 1) Economic-Cost-Driven Risk, focusing on expected mitigation costs [6], and 2) Physical-Security-Driven Risk, focusing on the intrinsic severity of contingencies using data-driven motifs [7] or advanced risk measures like Entropic Value-at-Risk [8].

While these approaches advance risk-informed dispatch, they have not yet fully addressed how to effectively coordinate multiple, concurrent physical risks within the same operational framework. This is particularly relevant in modern power systems where operational decisions must simultaneously guard against two growing threats: branch thermal overload risk and system frequency risk. On the one hand, concentrated high-power loads threaten to overburden critical branches; on the other, high renewable penetration erodes system inertia and challenges frequency stability. These risks can converge, creating a scenario where branch outages and frequency collapse may compound each other. To address this gap, this paper proposes a dual-risk RB-ACOPF model that incorporates both branch power flow risk and system frequency risk. The principal contributions are threefold:

(1) A Dual-Risk Framework: We develop a dual-risk framework in RB-ACOPF, quantifying economic impact between the branch flow risk and the system frequency risk. This integration yields marginal risk costs, revealing the economic interplay between these two security dimensions and moving beyond rigid, single-risk or deterministic criteria.

(2) An Endogenous, Optimization-Based Risk for Branch Security: We abandon the use of pre-defined, empirical severity indices for branch outages. Instead, we introduce a novel α-based severity assessment, where the branch flow risk is formulated as an endogenous model parameter. This provides a system-driven measure of structural vulnerability, making the risk assessment an integral part of the optimization rather than a subjective input.

(3) A Frequency Risk Formulation for Low-Inertia Systems: We translate the traditionally rigid frequency security con-

979-8-3315-8138-1

straints into a manageable frequency risk threshold. This reformulation improves flexibility and maintains security guarantees for low-inertia scenarios where conventional N-1 methods fail, offering a practical tool for future grids.

Numerical studies on IEEE 9-bus and 39-bus systems validate the effectiveness of model in navigating security-economic trade-offs.

II. Severity Calculation Criteria

In risk-based operational frameworks, the accurate estimation of contingency probability and severity is paramount. While outage probabilities can be derived from historical data or weather models, quantifying the severity of contingencies has traditionally relied on pre-defined empirical indices, which may lack clear physical interpretability. To overcome this limitation, we propose a novel optimization-based approach for severity assessment, as detailed below.

A. Severity of power flow risks

We propose an optimization-based "α-computation" that endogenously quantifies line criticality from the system structural and operational constraints. For each branch, we introduce a continuous variable α (0≤α≤1) that scales its thermal limit. Physically, α represents how much the capacity can be reduced without violating system feasibility. A value near 1 indicates the line is critical to system-wide feasibility and less expendable, whereas a lower α suggests its outage would cause less severe power-flow redistribution.

The objective minimizes the sum of the infinite-norms of α, thereby focusing on limiting the largest α-values. This approach prioritizes identifying and relieving the most critical thermal bottlenecks collectively, moving beyond predefined severity indices.

$$\min \sum \left\| \alpha_{ij} \right\|_{\infty}$$

Subject to

$$\begin{cases} P_i - V_i \sum_{j \in i} V_j (G_{ij}\cos\theta_{ij} + B_{ij}\sin\theta_{ij}) = 0 \\ Q_i - V_i \sum_{j \in i} V_j (G_{ij}\sin\theta_{ij} + B_{ij}\cos\theta_{ij}) = 0 \end{cases} \quad \forall i, j \in N \tag{1}$$

$$V_i^{\min} \le V_i \le V_i^{\max} \quad \forall i \in N \tag{2}$$

$$\left| S_{ij} \right| \le \alpha_{ij} S_{ij}^{\max} \quad \forall i, j \in N \tag{3}$$

$$\begin{cases} P_i^{\min} \le P_i \le P_i^{\max} \\ Q_i^{\min} \le Q_i \le Q_i^{\max} \end{cases} \quad \forall i \in G \tag{4}$$

The α values reflect branch criticality, a relationship further supported by the feasible region analysis in Section III.C. Since these values are derived from the system topology and a fixed load condition, they remain stable during the intra-day scheduling horizon and can thus be pre-computed as constant parameters. This design separates structural vulnerability assessment from the real-time dispatch optimization, thereby reducing the online computational complexity of the RB ACOPF.

B. Severity of system frequency risks

In contrast to the power flow risks associated with line outages, frequency-related security issues are more intimately linked with generator failures. Generator failure can cause an instantaneous power deficit, leading to a sudden drop in system frequency. In severe cases, this may trigger cascading failures. Consequently, the calculation of frequency risk severity necessitates the consideration of two key factors: the rate of change of frequency (RoCoF) and the frequency nadir.

The maximum RoCoF following a power imbalance is derived from the swing equation. To prevent under-frequency load shedding or generator protection tripping, the RoCoF must not exceed a predefined maximum value (e.g., $\mathrm{RoCoF}_{\max}$ =1 Hz/s). This leads to a constraint on the maximum allowable power imbalance $\Delta P_{\max}$:

$$RoCoF = \frac{\Delta P}{M} \tag{5}$$

$$\Delta P_{\max} \le M \cdot RoCoF_{\max} \tag{6}$$

The frequency nadir, the maximum allowable frequency drop, depends on both the system inertia and the responsive reserves. The constraint to maintain the nadir above a threshold $\Delta f_{\max}$ is given by:

$$H_{total} \cdot R_{total} \ge \frac{P_0^2 T_d}{4\Delta f_{\max}} \tag{7}$$

Where P_0 is the loss of the generator, H_{total} is the system inertia, R_{total} is available spinning reserve, and T_d is its delivery time, M is the inertia constant of the system (MWs/HZ). This shows that the severity of the disturbance impacts the nadir quadratically [9].

For system frequency security, the deterministic N-1 approach is generally applicable only to systems with sufficient inertia, as discussed in detail in Section IV. In contrast, the risk-based method quantifies frequency-related security metrics as risk values. This framework assigns a risk contribution for any predicted violation of security thresholds (RoCoF, nadir), while crediting risk mitigation for system components operating within safe limits. The overall system is deemed secure if the aggregated frequency risk remains below an acceptable threshold, providing a more flexible security assessment compared to deterministic pass/fail criteria.

III. Risk-based OPF Model

A. Mathematical Model

1) Variables and Parameters

Decision Variables:

$P_{Gi}, Q_{Gi}, V_i, \theta_i$: Conventional ACOPF decision variables

R_i : Spinning reserve provided by generator

Parameters:

$p_{ij}^{out}, p_{Gk}^{out}$: Outage probability of branch and generator

α_{ij} : Pre-computed severity coefficient for branch $i-j$

$S_{ij}^{\max}$: Apparent power thermal limit of branch $i-j$

φ_{ij} : Loading rate of branch, defined as $\sqrt{P_{ij}^2 + Q_{ij}^2} / S_{ij}^{\max}$

f_n, H_k : System frequency and total inertia without generator k

T_d : Delivery time of spinning reserve

$RoCoF_{\lim}, Nadir_{\lim}$: Security limits for frequency

ω_1, ω_2 : Weighting factors for RoCoF and nadir severity

λ_B, λ_F : Acceptable risk for branch flow risk and frequency risk

R_i^{max}, R_i^{max} : Minimum and maximum available spinning reserve

The Branch severity is quantified as $Sev_{ij} = \alpha_{ij} \cdot S_{ij}^{max}$. The risk contribution of each branch is:

$$Risk_{ij} = p_{ij}^{out} \cdot Sev_{ij} \cdot \varphi_{ij} \tag{8}$$

The risk from generator outage is a function of the resulting frequency deviation. The severity is a weighted sum of RoCoF and nadir violations:

$$Sev_{freq,k} = \omega_1 \cdot \left(RoCoF_k - RoCoF_{\lim} \right) + \omega_2 \cdot \left(Nadir_k - Nadir_{\lim} \right) \tag{9}$$

Where $RoCoF_k = \dfrac{P_{Gk} \cdot f_n}{2H_k}$, $Nadir_k = \dfrac{P_{Gk}^2 \cdot T_d}{4H_k \cdot R_k}$. The risk contribution of each generator is:

$$Risk_{freq,k} = p_{Gk}^{out} \cdot Sev_{freq,k} \cdot P_{Gk} \tag{10}$$

2) Objective Function

The objective is to minimize the total expected operational cost, which is the sum of the generation cost and the reserve cost:

$$\min \sum_i (C_i(P_{Gi}) + C_i^R(R_i))$$

3) Constraints

AC Power Flow Equations:

$$\begin{cases} P_i - V_i \sum_{j \in i} V_j (G_{ij} \cos\theta_{ij} + B_{ij} \sin\theta_{ij}) = 0 \\ Q_i - V_i \sum_{j \in i} V_j (G_{ij} \sin\theta_{ij} + B_{ij} \cos\theta_{ij}) = 0 \end{cases} \quad \forall i, j \in N \tag{11}$$

$$V_i^{min} \le V_i \le V_i^{max} \quad \forall i \in N \tag{12}$$

$$\begin{cases} \left| S_{ij} \right| \le S_{ij}^{max} \\ \left| S_{ji} \right| \le S_{ji}^{max} \end{cases} \quad \forall i, j \in N \tag{13}$$

Generator Limits:

$$\begin{cases} P_{Gi}^{min} \le P_{Gi} \le P_{Gi}^{max} \\ Q_{Gi}^{min} \le Q_{Gi} \le Q_{Gi}^{max} \\ R_i^{min} \le R_i \le R_i^{max} \\ \sum_{i \in G} R_i \ge \max P_{Gi} \end{cases} \quad \forall i \in G \tag{14}$$

Dual-Risk Constraints:

$$\sum_{(i,j) \in \ell} Risk_{ij} \le \lambda_B \tag{15}$$

$$\sum_{k \in G} Risk_{freq,k} \le \lambda_F \tag{16}$$

In summary, the proposed dual-risk ACOPF model extends the conventional ACOPF by integrating two risk constraints: branch power flow risk (15) and system frequency risk (16). A distinction of our risk quantification lies in its state-dependent formulation: both the branch loading rate and the generator output are functions of the dispatch decision variables. This represents a shift towards a dynamic, state-dependent risk quantification, moving away from a reliance on static, pre-defined values.

B. Solution Methodology

The procedure follows steps:

Step 1. Data and parameter initialization: Load the power system case data (e.g., network topology, generator parameters) and initialize parameters.

Step 2. α-computation: Solve the α-optimization model (1)-(4) to obtain the endogenous severity for each branch. This step is performed once as a preprocessing stage.

Step 3. RB ACOPF calculation: Solve the full RB-ACOPF model (11)-(16) using the severity indices from Step 2 and initial risk thresholds λ_B , λ_F .

Step 4. Adjust the risk thresholds iteratively: tighten them if system risk is high, or relax them to improve economics, until convergence. This step can be automated or guided by operator preference.

Step 5. Dispatch determination: Output the final generation dispatch, reserve capacity schedule, and associated system risk metrics that satisfy the operational and risk tolerance criteria.

The model is solved in Julia using IPOPT 3.14.17 with the MUMPS 5.7.3 solver, under a strict tolerance of 1e-6. To enhance convergence reliability, initialization is performed via a QGS-based method [10]. Key operational trends are consistent across all risk-threshold scenarios (Section IV, Tables II–VI), suggesting these insights are inherent to the proposed framework rather than artifacts of initial points or solver settings.

C. Feasible Region Analysis

The two risks mentioned in the model are based on thermal limit constraints and system frequency, respectively. As both are directly related to the active power of the system, the validity of the proposed method is verified from the perspective of the active power feasible region. A detailed description of feasible region characterization methods can be found in [11].

1) Branch Power Flow Severity:

This risk originates from line-outage contingencies. The coefficient α obtained from the α-computation reflects the tightness thermal limit of a branch within the system-wide system constraints. A higher α indicates that the branch is more critical; its outage would force substantial redirection of power flow, raising the risk of overloads elsewhere.

We examine changes in the active-power feasible region after disconnecting branches in the 39-bus system (Fig. 1a). Table I lists the top seven branches ranked by severity (α·S). Disconnecting the top six high-α branches sequentially (e.g., Branches 46, 14, etc.) makes the feasible region disappear unless a small amount of load is shed (approximately 2–3%), as shown in Fig. 1b and 1c. In contrast, disconnecting a low-α branch (Branch 35) leaves the feasible region virtually unchanged (Fig. 1d). These results show that α quantifies criticality of a branch to system feasibility. The drastic shrinkage or loss of the feasible region following the outage of a high-α branch indicates the severe post-contingency redistribution that would occur. Thus, α provides a feasibility-based measure of potential outage severity.

2) System Frequency Severity:

Frequency security presents a fundamental challenge in low-inertia systems, where generation loss can trigger rapid frequency deterioration. The 9-bus case study exemplifies this scenario, configured as a low-inertia system with all generators assigned an identical 3.25 s inertia constant. In such systems, a critical vulnerability emerges when a single generator supplies a disproportionately large load share. While economically efficient, this poses severe security risks: a failure of this dominant unit would cause a power deficit exceeding the system inertial resilience, leading to frequency violation. Our model addresses this through frequency risk constraints, which limit output from extreme but economically attractive units and redistribute generation to enhance security, as shown in Fig. 2 and 3. However, traditional N-1 deterministic methods fail to yield a feasible solution for this low-inertia system, even without considering voltage constraints. This shows that frequency security is a challenge in low-inertia scenarios, one that conventional approaches struggle to address.

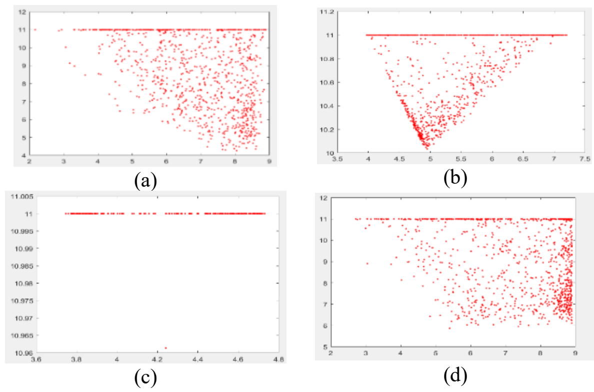

Figure 1 The feasible region (FR) for 39-bus system(a) Projection of initial feasible region. (b) FR after branch 46 is disconnected. (c) FR after branch 14 is disconnected. (d) (FR) after branch 35 is disconnected

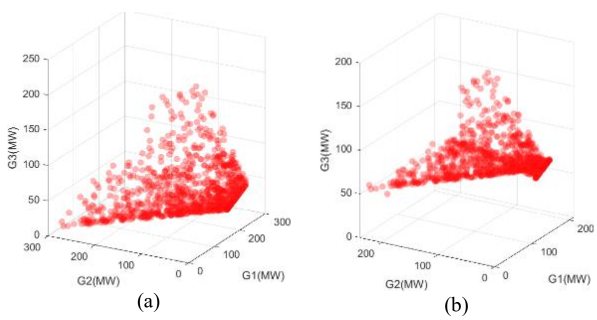

Figure 2. Feasible region for 9-bus system. (a)Without frequency risk. (b) With frequency risk. To secure frequency after generator loss, the model limits extreme unit outputs and balances generation, leading to a smaller but more secure and robust operational region for low-inertia systems.

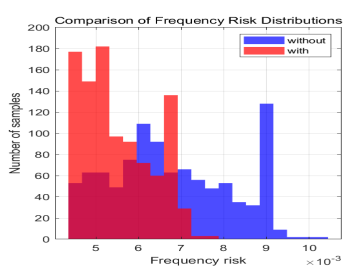

Figure 3 Comparison with and without frequency risk

IV. Case Studies and Numerical Results

The proposed model is illustrated using a 9-bus system. The system has 9 buses, 9 branches, 3 units, and 3 fixed loads. In this model, the outage probability of each branch is set to a fixed value of 0.2%, and the failure probability of each generator is set to 0.1% for simplicity. In practical applications, failure probability parameters estimated from historical data can be replaced by more sophisticated models to enhance predictive accuracy.

1) Branch Risk Dominant Regulation:

When the frequency risk threshold is set to a high value, system operation becomes predominantly governed by the branch flow risk constraint. The severity for critical branches is summarized in Table II. Tightening this constraint triggers a network-wide redistribution of power flows, primarily through the rescheduling of generation. For instance, the results illustrate this adjustment: the branch loading rate on Branch 4 (with the highest severity of 0.80) decreases, whereas that on Branch 5 (with the lowest severity of 0.42) increases correspondingly. This "risk transfer" phenomenon indicates the ability to identify and alleviate stress on the most vulnerable branches.

Table I Top 7 severity of branches in 39-bus system

Branch id	α·S (MW)	Feasibility
46	8.36	No
14	6.87	No
5	6.78	No
33	6.77	No
39	6.00	No
37	5.67	No
35	5.61	Yes

Table II Branch loading rates under different risk threshold (9-bus system)

Branch id	Branch risk		
	2.7e-3	2.6e-3	2.5e-3
	Loading rate (%)		
5	31.00	39.12	49.82
4	16.66	13.70	10.89

Table III Generation dispatch and reserve under different frequency risk threshold (9-bus system)

Unit id	Frequency risk					
	2.0e-3		1.0e-3		0.5e-3	
	output	reserve	output	reserve	output	reserve
G1	0.898	0.069	0.900	0.130	0.924	0.434
G2	1.344	0.060	1.340	0.060	1.302	0.098
G3	0.942	0.060	0.944	0.117	0.958	0.406
Cost ($)	5306.09		5312.51		5346.75	

2) Frequency Risk Dominant Regulation:

Conversely, under a low branch risk threshold, system security is dominated by the frequency risk constraint. Key parameters for frequency security, such as risk thresholds and reserve costs, are listed in Table III. As the frequency risk threshold is tightened, the model responds with a distinct two-stage adjustment strategy. The primary adjustment involves reserve capacity. Given its relatively lower cost, dispatching reserves is an economically efficient way to meet frequency security requirements. Secondary adjustment is generation dispatch: Once the reserve capacity of individual units approaches their upper limits, the model resorts to adjusting the power output of generators. To mitigate the impact of the most severe single-generator outage, the output is redistributed to become more balanced across all units. This "risk-spreading" strategy reduces the maximum possible power deficit from any single unit.

979-8-3315-8138-1

Table IV Total cost for dual risks under different threshold (9-bus system)

Branch risk	2.8e-3	2.7e-3	2.6e-3
Frequency risk	2.0e-3	1.3e-3	0.7e-3
Cost ($)	5321.2	5518.5	6061.8

Table V Total cost for dual risk under different threshold (39-bus system)

Branch risk	1.75e-1	1.70e-1
Frequency risk	4.00e-3	3.00e-3
Cost ($)	139495.3	140992.7

Table VI Model comparison in 9-bus system

Model	Branch security constraints	Frequency security constraints	Feasibility	Freq. Nadir (Hz)	Branch load rate diff (%)
N-1 ACOPF	×	×	√	1.16	27.54
N-1 ACOPF	×	√	×	-	-
RB-ACOPF1	√	×	√	1.38	18.04
RB-ACOPF2	×	√	√	0.29	27.32
Proposed RB-ACOPF	√	√	√	0.22	18.05

3) Co-regulation of dual risks and performance:

The interplay between both risks under simultaneous constraints reveals their relative marginal costs and scalability of the model (Table IV). The marginal cost of enhancing frequency security, primarily through reserve capacity deployment, is lower than that of enhancing branch power flow security, which requires costlier generation re-dispatch and network-wide power flow reshaping. This economic disparity underpins operational flexibility of the model: it preferentially satisfies frequency risk constraints via cheaper reserves before resorting to expensive generation shifts for branch risk management. Findings from the larger 39-bus system (Table V) are consistent with these principles. Due to ample system resources (e.g., more dispatchable branches and generators), tightening risk thresholds in this larger network has a negligible impact on total cost, indicating the capability of the model to navigate security-economic trade-offs in complex networks.

To systematically evaluate the advantages of the proposed dual-risk RB-ACOPF, we compare its performance against several benchmark models in the 9-bus system in Table VI. The N-1 ACOPF considering frequency security constraints fails to obtain a feasible solution in this low-inertia 9-bus system, highlighting the inadequacy of deterministic methods in the low-inertia system. Single risk RB-ACOPF1 and RB-ACOPF2 models succeed in mitigating one type of risk but leave the system exposed to the other. Notably, RB-ACOPF1 results in an unacceptably high frequency nadir (1.38 Hz), which can trigger under-frequency load-shedding protections. Conversely, RB-ACOPF2 leads to a high branch loading rate difference (difference between maximum and minimum load rate of branches), indicating unbalanced power flow that could cause unbalanced thermal overflows. In contrast, the proposed dual-risk RB-ACOPF is designed to provide joint security against both threats. It achieves the best frequency nadir (0.22 Hz) while maintaining a low and evenly distributed branch loading profile (18.05%), indicating its capability in coordinating both risks without compromising overall system security.

V. Conclusion

This paper has proposed a dual risk-based ACOPF framework. This framework is designed for power system operators in control centers, primarily for intra-day security-economic dispatch. The key contributions offer advances for grid operation: (1) A dual-risk framework that quantifies the economic impact between branch and frequency security, moving beyond single-risk or deterministic methods. (2) An endogenous α-computation for branch risk that replaces empirical indices with an optimization-driven measure of structural vulnerability. (3) A frequency risk formulation that transforms rigid constraints into manageable thresholds, thereby addressing low-inertia scenarios where conventional N-1 OPF fails.

Validation on test systems confirms the ability of the framework to balance security and economics. To further empower operators with flexible decision-making, our future work will develop a multi-objective framework that directly reveals the Pareto trade-offs among cost, branch risk, and frequency risk.

References

[1] E. L. Barrett, K. Mahapatra, M. Elizondo, X. Fan, S. Davis, S. Newman, P. Royer, B. Vyakaranam, F. B. D. Reis, X. Ke, and J. Dagle, "A risk-based framework for power system modeling to improve resilience to extreme events", *IEEE Open Access J. Power Energy*, vol. 10, pp. 25–35, 2023.

[2] Z. Wang, A. Younesi, M. V. Liu, G. C. Guo, and C. L. Anderson, "AC optimal power flow in power systems with renewable energy integration: A review of formulations and case studies," *IEEE Access*, vol. 11, pp. 102681–102712, 2023.

[3] A. M. Stanković et al., "Methods for analysis and quantification of power system resilience," *IEEE Trans. Power Syst.*, vol. 38, no. 5, pp. 4774–4787, Sep. 2023

[4] M. Draz, F. Pagel, and S. Albayrak, "Probabilistic risk assessment in power systems with high wind energy penetration," *IEEE Access*, vol. 12, pp. 140097–140111, 2024.

[5] Q. Wang, J. McCalley, T. Zheng and E. Litvinov, "A Computational Strategy to Solve Preventive Risk-Based Security-Constrained OPF," *IEEE Trans. Power Syst.*, vol.28, no.2, pp.1666-1675, May 2013

[6] L. You, H. Ma, T. K. Saha, and G. Liu, "Risk-based contingency constrained optimal power flow with adjustable uncertainty set of wind power," *IEEE Trans. Ind. Inform.*, vol. 18, no. 2, pp. 996–1008, Feb. 2022.

[7] K. Zhou, I. Dobson, and Z. Wang, "The most frequent N-k line outages occur in motifs that can improve contingency selection," *IEEE Trans. Power Syst.*, vol. 39, no. 1, pp. 1785–1796, Jan. 2024.

[8] L. Xu, H. Zeng, N. Lin, Y. Yang, Q. Guo and H. V. Poor, "Entropic Value-at-Risk constrained optimal power flow considering distribution network outages during extreme events," *IEEE Trans. Power Syst.*, vol. 40, no. 1, 2025, pp. 1184-1187.

[9] W. Xu, Z. Chu, F. Capitanescu and F. Teng, "On the Incorporation of Stability Constraints into Sequential Operational Scheduling," *2025 IEEE Power & Energy Society General Meeting (PESGM)*, Jul. 2025, pp. 1-5.

[10] T. Li, H.-D. Chiang, and Z.-Y. Wang, "A Quotient Gradient System-Based Trust-Tech Method for Computing Solutions of Multiple/All Feasible Components of ACOPF Models: Theory and Methodology," *IEEE Trans. Power Syst.*, Early Access, doi: 10.1109/TPWRS. 2025.3624256.

[11] H. Chiang and C. Jiang, "Feasible Region of Optimal Power Flow: Characterization and Applications," *IEEE Trans. Power Syst.*, vol. 33, no. 1, pp. 236-244, Jan. 2018